Cell Death and Differentiation (2012) 19, 1413–1423

www.nature.com/cdd

Pivotal role of the RanBP9-cofilin pathway in Aβ-induced apoptosis and neurodegeneration

JA Woo[1], AR Jung[1], MK Lakshmana[2], A Bedrossian[2], Y Lim[1], JH Bu[2], SA Park[2], EH Koo[2], I Mook-Jung[1] and DE Kang*[,1,2]

Neurodegeneration associated with amyloid β (Aβ) peptide accumulation, synaptic loss, neuroinflammation, tauopathy, and memory impairments encompass the pathophysiological features of Alzheimer's disease (AD). We previously reported that the scaffolding protein RanBP9, which is overall increased in brains of AD patients, simultaneously promotes Aβ generation and focal adhesion disruption by accelerating the endocytosis of amyloid precursor protein (APP) and β1-integrin, respectively. Here, we show that RanBP9 protein levels are increased by fourfold in FAD mutant APP transgenic mice. Accordingly, RanBP9 transgenic mice demonstrate significantly increased synapse loss, neurodegeneration, gliosis, and spatial memory deficits. RanBP9 overexpression promotes apoptosis and potentiates Aβ-induced neurotoxicity independent of its capacity to promote Aβ generation. Conversely, RanBP9 reduction by siRNA or gene dosage mitigates Aβ-induced neurotoxicity. Importantly, RanBP9 activates/dephosphorylates cofilin, a key regulator of actin dynamics and mitochondria-mediated apoptosis, and siRNA knockdown of cofilin abolishes both Aβ and RanBP9-induced apoptosis. These findings implicate the RanBP9–cofilin pathway as critical therapeutic targets not only for stemming Aβ generation but also antagonizing Aβ-induced neurotoxicity.
Cell Death and Differentiation (2012) **19,** 1413–1423; doi:10.1038/cdd.2012.14; published online 24 February 2012

Alzheimer's disease (AD) is a neurodegenerative disorder characterized by accumulations of the amyloid β (Aβ) -peptide and hyperphosphorylated tau in senile plaques and neurofibrillary tangles, respectively. Aβ is a neurotoxic peptide derived from β- and γ-secretase cleavages of the amyloid precursor protein (APP) and is thought to be a critical early player in AD pathogenesis.[1] In addition to the accumulation of Aβ and tau, abnormalities in the actin cytoskeleton are detected earlier during the course of AD and other neurodegenerative diseases.[2] Indeed, it has been demonstrated that Aβ can induce actin/cofilin pathology associated with hyperphosphorylated tau in primary neurons and *in vivo*.[3–5]

We recently demonstrated that the scaffolding protein RanBP9 interacts with the cytoplasmic tails of LRP, APP, and BACE1, and functions as a scaffold upon which APP is brought together with BACE1 and LRP. Such interactions of RanBP9 promote the endocytosis of APP and strongly increase BACE1 cleavage of APP to generate Aβ *in vitro* and *in vivo*.[6,7] Conversely, siRNA knockdown of RanBP9 reduces BACE1 cleavage of APP and Aβ generation, indicating that endogenous RanBP9 normally functions in this capacity.[6] In addition, a 60-kD proteolytic fragment of RanBP9 is increased by more than sixfold in brains of AD patients, and this fragment potentiates Aβ generation via BACE1 processing of APP.[8] In addition to promoting Aβ generation by accelerating APP endocytosis, RanBP9 also potently disrupts integrin-dependent focal adhesion signaling and assembly by accelerating β1-integrin and LRP endocytosis.[9] In this study, we found that RanBP9 levels are increased not only in brains of AD patients but also in APP transgenic mice. Increased RanBP9 expression significantly induces gliosis, neurodegeneration, synapse loss, and spatial memory deficits. Mechanistic studies demonstrate that RanBP9 activates cofilin and that both RanBP9 and cofilin are key intermediates of Aβ-induced cell death.

Results

Accumulation of RanBP9 protein in mutant APP transgenic mice and generation of RanBP9 transgenic mice. We previously demonstrated that the overall levels RanBP9, particularly the bioactive N-terminal 60 kD fragment (N60), is increased in brains of AD patients compared with the age-matched healthy controls.[8] Thus, we assessed whether RanBP9 levels might be altered in a mouse model of AD pathology. In brains of 10–12-month-old J20 APP transgenic mice carrying both the Swedish and Indiana APP mutations, RanBP9 levels were increased by more than fourfold in J20 mice compared with their non-transgenic counterparts (Figures 1a and b). As the J20 mice demonstrate substantial amounts of amyloid plaque accumulation at this age,[10] this indicates that APP and/or Aβ accumulation result in increased RanBP9 levels.

[1]WCU-Neurocytomics Program, Seoul National University College of Medicine, Seoul, Korea and [2]Department of Neurosciences, University of California, San Diego, La Jolla, CA, USA
*Corresponding author: DE Kang, Department of Neurosciences, University of California, San Diego, Leichtag Biomedical Research 375, 9500 Gilman Drive, La Jolla, CA 92093, USA. Tel: +1 858 519 7081; Fax: +1 858 822 1021; E-mail: dekang@ucsd.edu
Keywords: amyloid; RanBP9; cofilin; apoptosis; synapse; gliosis
Abbreviations: RanBP9, Ran-binding protein 9; APP, amyloid precursor protein; LRP, low-density lipoprotein receptor-related protein; GFAP, glial fibrillary acidic protein; BACE1, beta site APP-cleaving enzyme 1; LDH, lactate dehydrogenase; AD, Alzheimer's disease; FAD, familial Alzheimer's disease; DIV, days *in vitro*; PSD95, postsynaptic density 95; TUNEL, terminal uridine nick-end labeling; FACS, fluorescence-activated cell sorter; LIMK, LIM kinase; IML, inner molecular layer; SL, stratum lucidum; ADF, actin-depolymerizing factor; PTP, permeability transition pore; PI, propidium iodide
Received 05.9.11; revised 27.12.11; accepted 24.1.12; Edited by L Greene; published online 24.2.12

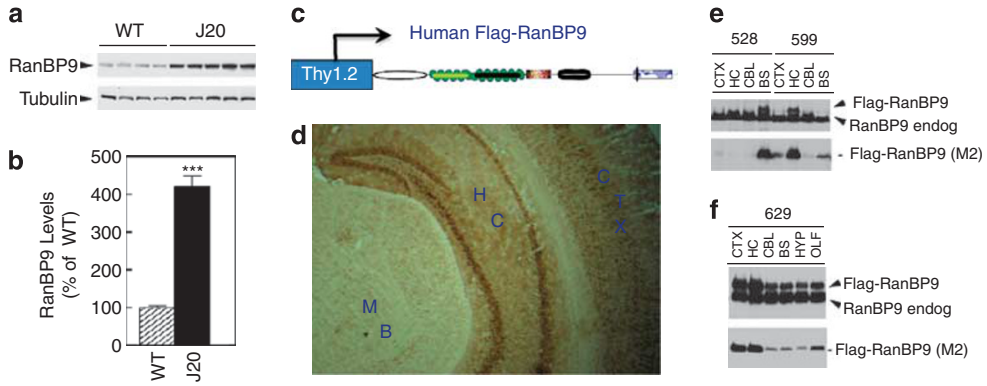

Figure 1 Increased RanBP9 levels in mutant APP transgenic mice and expression profile of human Flag-RanBP9 transgenic mice. (**a**) Brain homogenates from 10- to 12-month-old J20 mice (APP695 carrying the Swedish and Indiana mutations) and non-transgenic littermates were subjected to SDS-PAGE and immunoblotting for RanBP9 protein. (**b**) Quantitation of RanBP9 protein normalized to tubulin demonstrates a highly significant increase in RanBP9 protein levels in J20 mice (***$P<0.0001$, $t=10.8$, $df=7$). (**c**) Schematic representation of human Flag-RanBP9 transgene driven by the mouse Thy1.2 promoter. (**d**) Expression of the Flag-RanBP9 transgenic protein detected by the M2 Flag antibody from a 3-month-old line 629 RanBP9 transgenic mice. Immunohistochemical expression profile shows extensive expression of Flag-RanBP9 in the midbrain (MB) hippocampus (HC) and cortex (CTX). (**e** and **f**) Different regions of the brain including cortex (CTX), hippocampus (HC), cerebellum (CBL), and brain stem (BS) were dissected from line 528 and 599 mice and line 629 mice and subjected to immunoblotting for endogenous RanBP9 and transgenic Flag-RanBP9 using anti-RanBP9 antibody (upper panel) and M2 antibody (lower panel). Note the highest expression of Flag-RanBP9 in the hippocampus and cortex of line 629 transgenic mice

To determine whether experimentally increasing RanBP9 levels in transgenic mice would produce pathological consequences in brain, we generated several lines of hemizygous RanBP9 transgenic mice (lines 528, 599, and 629) using the mouse Thy-1.2 promoter to drive neuronal expression of human Flag-RanBP9 (Figure 1c, Supplementary Methods). As shown in Figure 1, the human Flag-RanBP9 migrated slightly slower than the endogenous RanBP9. Line 528 only expressed Flag-RanBP9 in the brain stem (BS), whereas line 599 expressed Flag-RanBP9 mostly in the hippocampus, with only small amounts in the cortex (ctx) and BS (Figures 1e and f). Line 629 expressed the highest amount of Flag-RanBP9 (about twofold excess), especially in the ctx and hippocampus, with moderate amounts in the cerebellum (cbl), BS, hypothalamus (hyp) (Figure 1d), and olfactory bulb (olf) (Figure 1f).

For the initial analysis of line 629 RanBP9 transgenic mice, we used an antibody microarray approach in six 1-year-old transgenic mice brains and six of their respective non-transgenic littermates to identify clues to any proteins or signaling pathways that might be altered as a consequence of increased RanBP9 expression. From this analysis, we found significant alterations in cell death pathways, neuroinflammatory responses, cell cycle proteins, and focal adhesion signaling (Supplementary Table S1).

RanBP9 induces hippocampal gliosis associated with synapse loss and neurodegeneration *in vivo*. We examined 1-year-old line 629 RanBP9 transgenic mice and non-transgenic littermates for the signs of neuroinflammation by immunohistochemical analysis of GFAP (astrogliosis) and Iba-1 (microgliosis). As predicted, both GFAP and Iba-1 immunoreactivities were saliently increased in the hippocampus of RanBP9 transgenic mice compared with the non-transgenic littermate controls (Figure 2a). Specifically, the robust increase in Iba-1 immunoreactivity was clearly evident beneath the hippocampal fissure where the perforant path forms connections with dendrites of the dentate gyrus and CA3, suggesting degeneration of dendritic/axonal processes that connect within this region (Figure 2a). Quantitation of Iba-1-positive microglia from the entire hippocampus demonstrated a highly significant ~2.5-fold increase in RanBP9 transgenic mice compared with the non-transgenic littermates (Figure 2b, $n=4$ each, $P<0.0015$). In addition, quantitation of GFAP-positive astrocytes showed ~twofold increase in RanBP9 transgenic mice compared with the non-transgenic littermates (Figure 2c, $n=4$ each, $P<0.001$). The increase in GFAP-positive astrocytes was clearly evident throughout the hippocampus, especially stratum radiatum where Schaffer collateral fibers form connections with CA1 and CA3 (Figure 2a). Moreover, the shape of the GFAP-positive astrocytes appeared to be much more activated in RanBP9 transgenic mice compared with littermate controls, with elongated processes and star-shaped appearance (Figure 2a). Taken together, these data demonstrate that increased expression of RanBP9 leads to neuroinflammation of both microglia and astrocytes probably associated with dendritic/synaptic damage within the hippocampus.

Given the observed neuroinflammation in RanBP9 transgenic mice, we next assessed whether synapses are altered as a consequence of increased RanBP9 expression *in vivo*. To this end, we examined synaptophysin immunoreactivity within various synaptic terminal zones of the hippocampus. Although we did not detect significant differences within the CA1 area of the hippocampus (not shown), we observed a highly significant reduction in the synaptophysin immunoreactivity within the stratum lucidum (SL) of CA3 (granule cell terminating zone; $P<0.0023$; Figures 2e and g) and within the inner molecular layer (IML, hilar mossy cell terminating zone) of the dentate gyrus ($P<0.0074$; Figures 2e and g) of RanBP9 transgenic mice. Synaptophysin levels were similarly decreased in the hippocampus of RanBP9 transgenic mice by immunoblotting ($P<0.0051$, Figures 3e and f). We also

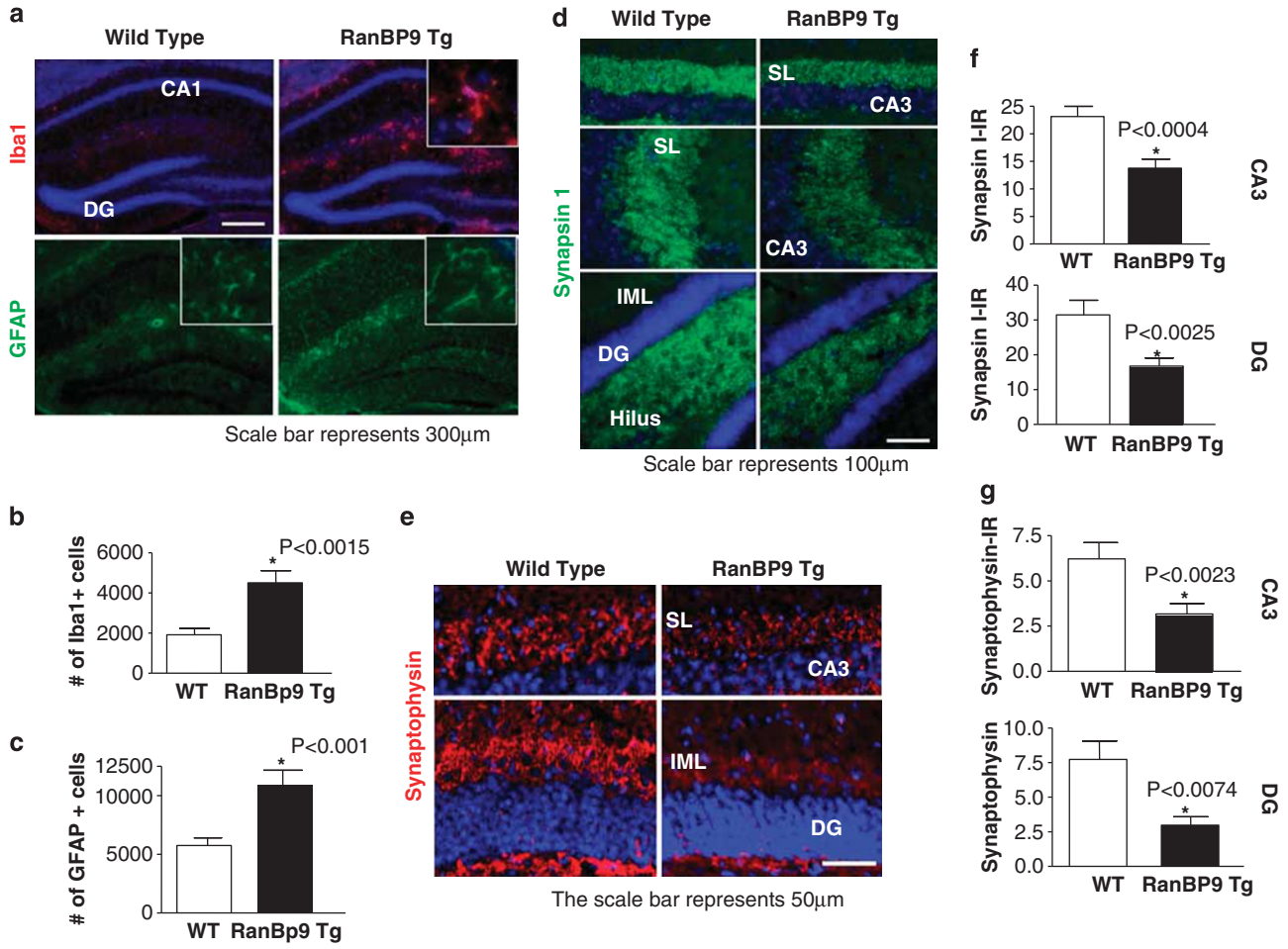

Figure 2 Markedly increased gliosis and synapse loss in the hippocampus of RanBP9 transgenic mice. (**a**) Cryosections from 1-year-old RanBP9 transgenic mice ($n=4$) and wild-type littermates ($n=4$) were subjected to immunohistochemistry for Iba1 (microglial marker, upper panels) and GFAP (astrocytic marker, lower panels) and counterstained with DAPI (blue). Representative immunostains are shown. Note the highly activated form of microglia and astrocytes in the hippocampus of RanBP9 transgenic mice (insets magnified $\times 12$). (**b** and **c**) Quantitation shows a highly significant increase in Iba1-positive microglia ($P<0.0015$) and GFAP-positive astrocytes ($P<0.001$) in the hippocampus of RanBP9 transgenic mice. (**d** and **e**) Cryosections from 1-year-old RanBP9 transgenic mice ($n=4$) and wild-type littermates ($n=4$) were subjected to immunohistochemistry for synapsin I (green) or synaptophysin (red) and counterstained with DAPI (blue). Representative immunostains of CA3 and dentate gyrus of the hippocampus are shown. (**f** and **g**) Synaptophysin, a synapsin I immunoreactivities were determined by quantifying the density of presynapses of stratum lucidum (SL) of CA3 (granule cell mossy fiber terminating zone) and inner molecular layer (hilar mossy cell-terminating zone; for synaptophysin) or hilus (for synapsin I) of the dentate gyrus using Image J software. Note the highly significant reductions in synaptophysin and synapsin I immunoreactivities in the CA3 (synaptophysin, $P<0.0023$; synapsin I, $P<0.0004$) and dentate gyrus (synaptophysin, $P<0.0074$; synapsin I, $P<0.0025$) of RanBP9 transgenic mice

assessed another presynaptic marker, synapsin I, known to function in synaptogenesis. Similar to that seen with synaptophysin, synapsin I immunoreactivity was significantly reduced in both the CA3 and hilus of the dentate gyrus of RanBP9 transgenic mice compared with littermate controls (Figures 2d and f). Interestingly, synapsin I immunoreactivity was not detected in the IML of dentate gyrus but rather concentrated in the hilus (Figure 2d), suggesting that these synapses are distinct from those containing synaptophysin. Consistent with the observed synaptic loss, TUNEL-positive-condensed nuclei were markedly increased throughout the hippocampus of RanBP9 transgenic mice (Supplementary Figure S1). In primary hippocampal neurons derived from postnatal day 0 (P0) RanBP9 transgenic mice and grown to 21 days *in vitro* (DIV), we also observed significant reductions in both synaptophysin (presynaptic) and PSD95 (postsynaptic) immunoreactivities compared with control littermates (Figures 3a–d). Therefore, these results indicate that RanBP9 mediates synaptotoxicity as early as DIV21 in primary neurons as well as synaptic damage and neurodegeneration *in vivo*.

RanBP9 impairs spatial learning and memory. Given the synaptic loss, neurodegeneration, and neuroinflammation observed in RanBP9 transgenic mice, we assessed 1-year-old RanBP9 transgenic mice and non-transgenic littermates in a variety of behavioral tasks. We did not observe any significant differences in rearing, center activity, ambulation, or total horizontal activity between RanBP9 transgenic mice and non-transgenic littermates (Supplementary Figure S2), indicating that RanBP9 does not influence locomoter activity. Next, we tested the mice in Barne's maze, a spatial learning and memory task that require proper hippocampal function.

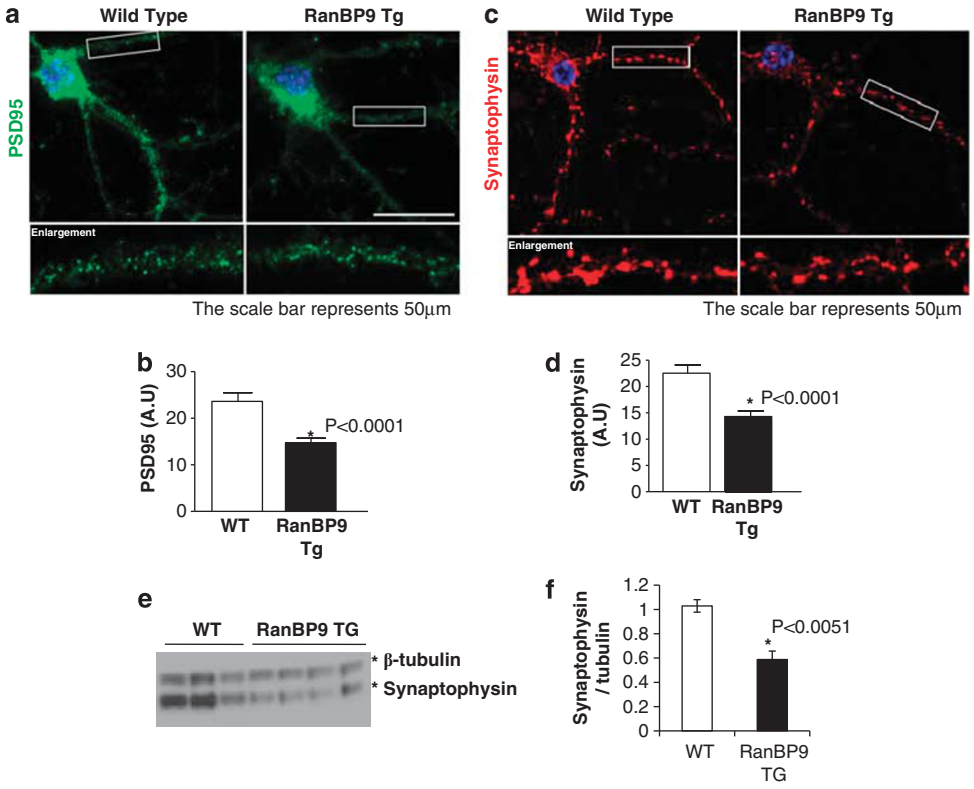

Figure 3 Significant reductions in PSD95 and synaptophysin immunoreactivities in RanBP9 transgenic primary hippocampal neurons. (**a** and **c**) P01 primary hippocampal neurons were cultured from wild-type and RanBP9 transgenic mice and stained for PSD95 (postsynaptic) or synaptophysin (presynaptic) at DIV21. Representative images are shown. (**b** and **d**) Quantitations of synaptophysin and PSD95 immunoreactivites demonstrate significantly reduced intensities of PSD95 ($P<0.0001$) and synaptophysin ($P<0.0001$). Error bars represent S.E.M. (**e**) Hippocampal brain extracts from three 1-year old wild-type and four 1-year old RanBP9 transgenic mice were subjected to immunoblotting for synaptophysin and β-tubulin. (**f**) Densitometric quantitation of synaptophysin normalized to β-tubulin shows a significant reduction in synaptophysin in RanBP9 transgenic hippocampi compared to those of non-transgenic littermates ($P<0.0051$)

Upon presentation of bright light and loud noise, mice were trained to locate an escape tunnel for 12 sessions. Although RanBP9 transgenic mice were somewhat slower in learning the location of the escape tunnel than wild-type mice, both mouse genotypes eventually learned the Barne's maze task (Figure 4a). After the 12th training session, the escape tunnel was removed and the amount of time mice spent in each quadrant was measured in a probe trial. Therefore in this paradigm, the amount of time spent in the quadrant where the escape tunnel was located is a measure of true spatial memory without regard to olfactory cues or other learning strategies. Wild-type mice spent ~60% of the time in the target quadrant where the escape tunnel was located. However, RanBP9 transgenic mice only spent ~30% of the time in the target quadrant (Figures 4b and c), indicating that these mice did not learn the Barne's maze task in a spatial manner. Unlike the wild-type mice that progressively learned the location of the escape tunnel predominantly via a spatial strategy, RanBP9 transgenic mice relied primarily on a sequential entry strategy (Supplementary Figure S3). We next tested the mice in a Y-maze test for spontaneous alterations, a model for studying working memory in which mice tend to spontaneously explore all the three arms of the Y-maze. In this test, both wild-type and RanBP9 transgenic mice performed similar numbers of spontaneous alterations, indicating that the working memory of RanBP9 transgenic mice is not significantly impaired (Supplementary Figure S4).

To determine whether RanBP9 transgenic mice are impaired in another spatial memory task, we next assessed the mice in the contextual fear-conditioning test. On day 1, mice were placed in the conditioning chamber for 5 min to habituate them to the apparatus. During the habituation phase, there were no observable differences between the wild-type and RanBP9 transgenic mice in the amount of freezing behavior (Figure 8). On day 2, mice were exposed to the context and conditioned stimulus in association with foot shock. On day 3, contextual conditioning was measured by the amount of freezing behavior in a 5 min session. Although wild-type mice froze for an average of more than 61 s, RanBP9 transgenic mice froze for less than 6 s, indicating that the latter mice did not remember the context in which they were placed (Figure 4d). On day 4, mice were tested for cued conditioning (CS + test) in a chamber disguised with new walls and floor (black opaque) and a new odor. Mice were placed in the novel context for 3 min, after which they were exposed to the conditioned stimulus (tone), and freezing behavior was measured for 5 min. In this tone cued-conditioning test, both wild-type and RanBP9 transgenic mice froze for more than 50 s and did not differ significantly with each other (Figure 4d), indicating that they are both capable of

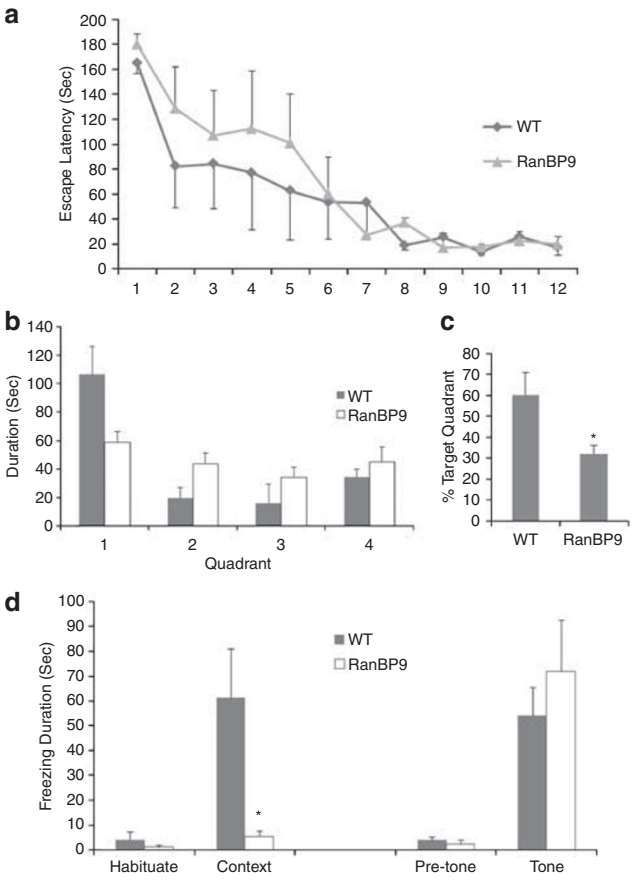

Figure 4 Impaired spatial memory in RanBP9 transgenic mice. (**a**) One-year-old RanBP9 transgenic mice ($n=4$) and wild-type littermates ($n=4$) were subjected to 12 sessions of Barne's maze testing. Escape latency represents the time to locate the escape tunnel. (**b** and **c**) For the 13th test (probe test), the escape tunnel was removed and the mouse was allowed to freely explore the maze for 3 min. The time spent in each quadrant was determined and the percent time spent in the target quadrant (the one originally containing the escape box) was compared with the average percent time in the other three quadrants. Note the significant reduction in the percentage of time spent in the target quadrant in RanBP9 transgenic mice ($^*P<0.05$, $t=2.51$, df $=6$), indicating impairment in spatial memory. (**d**) Mice were subjected to the contextual fear-conditioning test followed by the tone cued test (see methods). Freezing behavior in the context and cued tests is indicative of the contextual and cued memory, respectively. Note the severe reduction in freezing time in the contextual but not cued test in RanBP9 transgenic mice ($^*P<0.02$, $t=3.15$, df $=7$)

learning the association of tone with the shock. Taken together, these data demonstrate that RanBP9 transgenic mice are selectively impaired in hippocampus-dependent spatial memory tasks, consistent with the neuroinflammation, synapse loss, and neurodegeneration seen in these mice.

RanBP9 overexpression potentiates and RanBP9 reduction mitigates Aβ-induced apoptosis. Given the observed activation of cell death pathways and neurodegeneration in RanBP9 transgenic mice, we next assessed whether RanBP9 promotes cell death in a cell culture model. Under serum withdrawal conditions (2% serum) for 12 h in HT22 cells (hippocampus-derived neuroblastoma cell line),[9,11] RanBP9 transfection effectively doubled the number of cells at the early stages of apoptosis (lower right quadrant) as measured by Annexin V/PI staining and FACS (Supplementary Figure S5A). Similar to that seen in HT22 cells, RanBP9 or GFP-RanBP9 transfections doubled more than the amount of LDH release compared with the vector control or EYFP transfections in H4 neuroglioma cells (Supplementary Figures S5B and C).

Next, we tested whether manipulating RanBP9 levels alters toxicity in response to Aβ1–42 treatment. Aβ1–42 oligomers were prepared using the Klein method,[12,13] which demonstrated the presence of SDS-stable Aβ monomers, dimers, trimers, and tetramers in the absence of high molecular weight Aβ fibrils (Supplementary Figure S5D). Thus, HT22 cells were transfected with vector control or RanBP9 in regular 10% FBS-containing medium for 6 h, after which the medium was replaced with 1% FBS-containing medium for 24 h in the presence or absence of 1 μM Aβ1–42 oligomer preparations. Under this prolonged serum withdrawal condition in HT22 cells, the majority of cells were already in early apoptotic phase (lower right quadrant). RanBP9 transfection further increased early apoptotic cells even in the absence of Aβ1–42 (Figure 5a). The concentration of 1 μM Aβ1–42 oligomer preparations *per se* increased the number of cells in the early apoptotic phase (lower right quadrant) but did not appreciably increase cells in the late apoptotic phase (upper right quadrant) (Figure 5a). However, RanBP9 transfection more than doubled the conversion of early apoptotic cells (lower right quadrant) to late apoptotic cells (upper right quadrant) compared with the vector control transfection (Figure 5a). We next assessed whether reducing endogenous RanBP9 levels might protect from Aβ-induced cell death. For this purpose, HT22 cells were transfected twice with sense control siRNA or RanBP9-specific siRNA over a 56-h period (Supplementary Figure S6A). After the second transfection, the medium was replaced with 1% FBS-containing medium for 36 h in the presence or absence of 1 μM Aβ1–42 oligomers. Under these conditions, 1 μM Aβ1–42 in the presence of control sense siRNA increased the conversion of early apoptotic cells (lower right quadrant) to late apoptotic cells (upper right quadrant) (Figure 5b). However, transfection of RanBP9 siRNA nearly abolished this apoptotic process induced by Aβ1–42 (Figure 5b). To determine whether reduction in *RanBP9* gene dosage also protects from Aβ1–42-induced neurotoxicity in primary neurons, we cultured *RanBP9*+/− hippocampal neurons (Supplementary Methods) and those from wild-type control littermates at P0 and subjected them to treatment with 1 μM Aβ1–42 oligomers for 24 h on DIV14. In the absence of Aβ exposure, no detectable Annexin V or PI signals were observed in either wild-type or *RanBP9*+/− primary neurons (not shown). Aβ treatment dramatically increased both early (Annexin-positive, PI-negative) and late (Annexin/PI-double positive) cells in both wild-type and *RanBP9*+/− neurons (Figures 5c and d). However, *RanBP9*+/− neurons displayed greatly reduced sensitivity to Aβ treatment as both early (17% *RanBP9*+/− *versus* 28% WT) and late (25% *RanBP9*+/− *versus* 58% WT) apoptotic cells were significantly reduced (Figure 5c and d; $P<0.0001$). As expected, *RanBP9*+/− neurons expressed much reduced levels of endogenous RanBP9 protein (Figure 5e). These results indicate that

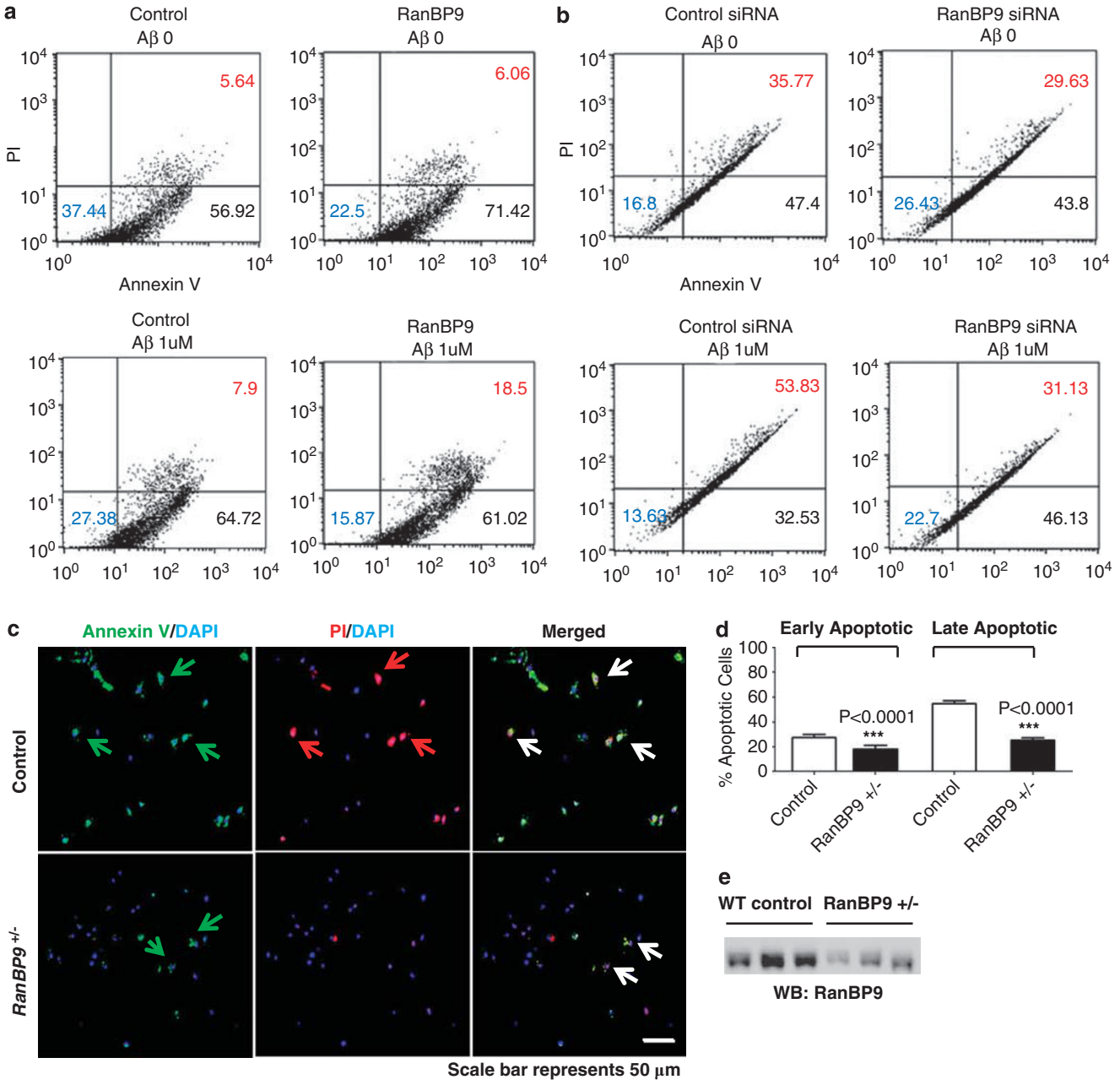

Figure 5 RanBP9 overexpression potentiates and RanBP9 reduction disrupts Aβ-induced apoptosis. (**a**) HT22 cells were transfected with vector control or RanBP9 in regular 10% FBS-containing medium for 6 h, after which the medium was replaced with 1% FBS-containing medium for 24 h in the presence or absence of 1 μM Aβ 1–42 oligomers. Cells were then subjected to FACS analysis after propidium iodide (PI: *Y*-axis) and Annexin V (*X*-axis) staining. Note that RanBP9 transfection increases early apoptotic cells even in the absence of Aβ1–42 and potentiates the conversion of early apoptotic cells (lower right quadrant) to late apoptotic cells (upper right quadrant). A representative experiment is shown from three independent experiments. (**b**) HT22 cells were transfected twice with sense control siRNA- or RanBP9-specific siRNA over a 56 h period. After the second transfection, the medium was replaced with 1% FBS-containing medium for 36 h in the presence or absence of 1 μM Aβ1–42. Cells were then subjected to FACS analysis after propidium iodide (PI: *Y*-axis) and Annexin V (*X*-axis) staining. Under these conditions, note that 1 μM Aβ1–42 increases the conversion of early apoptotic cells (lower right quadrant) to late apoptotic cells (upper right quadrant). However, transfection of RanBP9 siRNA nearly abolishes this apoptotic process. A representative experiment is shown from three independent experiments. (**c** and **d**) *RanBP9*+/− and wild-type littermate hippocampal primary neurons (DIV14) were treated with 1 μM Aβ1–42 oligomers for 24 h and subjected to staining for Annexin V (green) and PI (red) followed by DAPI (blue). Arrows indicate examples of Annexin V/PI double-positive cells (late apoptotic). Quantitation from three experiments show significantly reduced numbers of early (Annexin V-positive, PI-negative) and late (Annexin V/PI-double positive) apoptotic cells in *RanBP9*+/− neurons. Error bars represent S.E.M. (**e**) Western blotting of endogenous RanBP9 demonstrates reduced RanBP9 protein levels in *RanBP9*+/− neurons compared to wild-type littermate neurons

RanBP9 renders cells more vulnerable to Aβ-induced toxicity and that endogenous RanBP9 is an intermediate required for the full complement of Aβ-induced apoptosis.

RanBP9-induced cell death is independent of its capacity to promote Aβ generation. We previously showed that increased RanBP9 expression promotes

BACE1 processing of APP and Aβ generation by scaffolding APP/BACE1/LRP complexes together and accelerating APP endocytosis.[6] To determine whether RanBP9-induced cell death is dependent on its ability to promote Aβ generation, we treated HT22 cells with or without 5 μM γ-secretase inhibitor, DAPT, for 24 h under normal cell culture conditions (10% FBS). In the absence of Aβ oligomer treatment, no detectable Annexin V or PI staining could be observed in control empty vector-transfected cells in the presence or absence of γ-secretase inhibition (Figure 6). However, RanBP9 transfection alone significantly increased both early and late apoptotic cells both in the presence or absence of DAPT treatment (Figures 6c–f). Treatment of 1 μM Aβ1–42 oligomers greatly increased the numbers of early apoptotic cells in control vector-transfected cells, while RanBP9 transfection further potentiated Aβ-induced increase in early and late apoptotic cells regardless of γ-secretase inhibition. Parallel experiments confirmed the expected accumulation of APP-CTFs and no change in full length APP after γ-secretase inhibitor treatment (Supplementary Figure S6C). These results therefore indicate that the ability of RanBP9 to promote cell death in this paradigm is largely independent of its capacity to promote Aβ generation, although the latter process is expected to be additive in the AD brain.

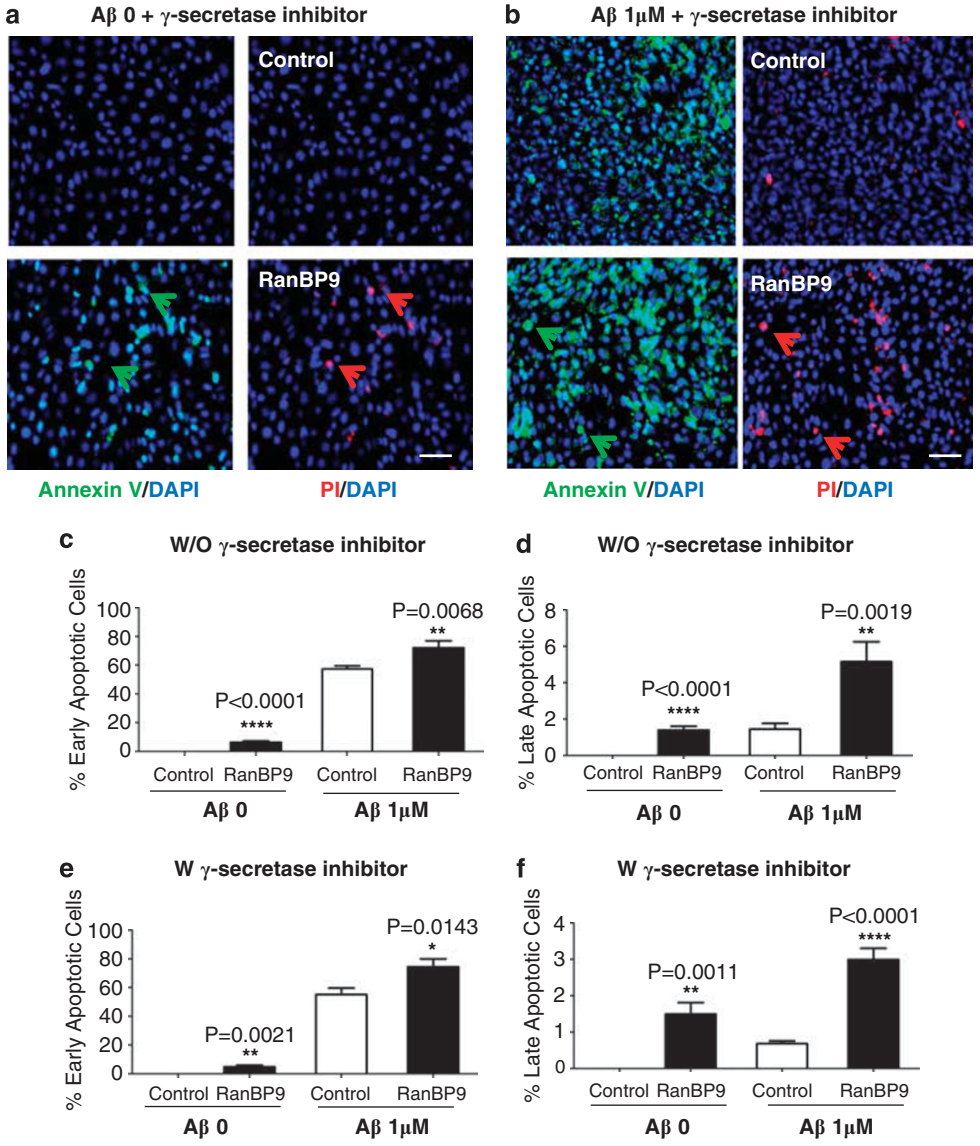

Figure 6 The ability of RanBP9 to induce cell death does not dependent on its capacity to promote Aβ generation. (**a** and **b**) HT22 cells were transfected with vector control or RanBP9 for 16 h, and treated with or without 1 μM Aβ1–42 oligomers in the presence or absence of 5 μM DAPT (γ-secretase inhibitor) for 24 h in normal medium (10% FBS). Cells were then subjected to staining for Annexin V (green) and PI (red) followed by DAPI (blue). A representative experiment from DAPT-treated cells is shown. Scale bar represents 50 μm. Arrows show examples of Annexin V and PI double-positive cells (late apoptotic). (**c–f**) Quantitation from three experiments shows that RanBP9 transfection alone significantly increases both early (Annexin V-positive, PI-negative) and late (Annexin V/PI-double positive) apoptotic cells in the presence or absence of γ-secretase inhibition, while RanBP9 also potentiates the effects of Aβ1–42 in promoting cell death regardless of γ-secretase inhibition. Comparisons are made between control- and RanBP9-transfected cells with or without Aβ1–42 treatment. Error bars represent S.E.M

Cofilin activation mediates Aβ- and RanBP9-induced apoptosis. We previously demonstrated that RanBP9 disrupts focal adhesion signaling and assembly by accelerating β1-integrin and LRP endocytosis.[9] Downstream of integrin engagement with the matrix and focal adhesion signaling, kinases such as Src and LIM kinase (LIMK) are activated, which results in the phosphorylation and deactivation of cofilin. The activity of cofilin is controlled by phosphorylation and dephosphorylation on serine-3 of cofilin by LIMK and Slingshot-1L (SSH), respectively.[14,15] Consistent with the role of RanBP9 in focal adhesion disruption,[9] cofilin levels were dramatically enhanced (Figures 7a and b), and serine-3 phosphorylated cofilin levels were reduced after RanBP9 transfection (Figure 7a). Therefore, RanBP9 significantly reduced the level of phospho-cofilin per total cofilin to less than 15% of control-transfected cells (Figure 7c). Immunofluorescence studies also demonstrated highly elevated levels of cofilin in RanBP9

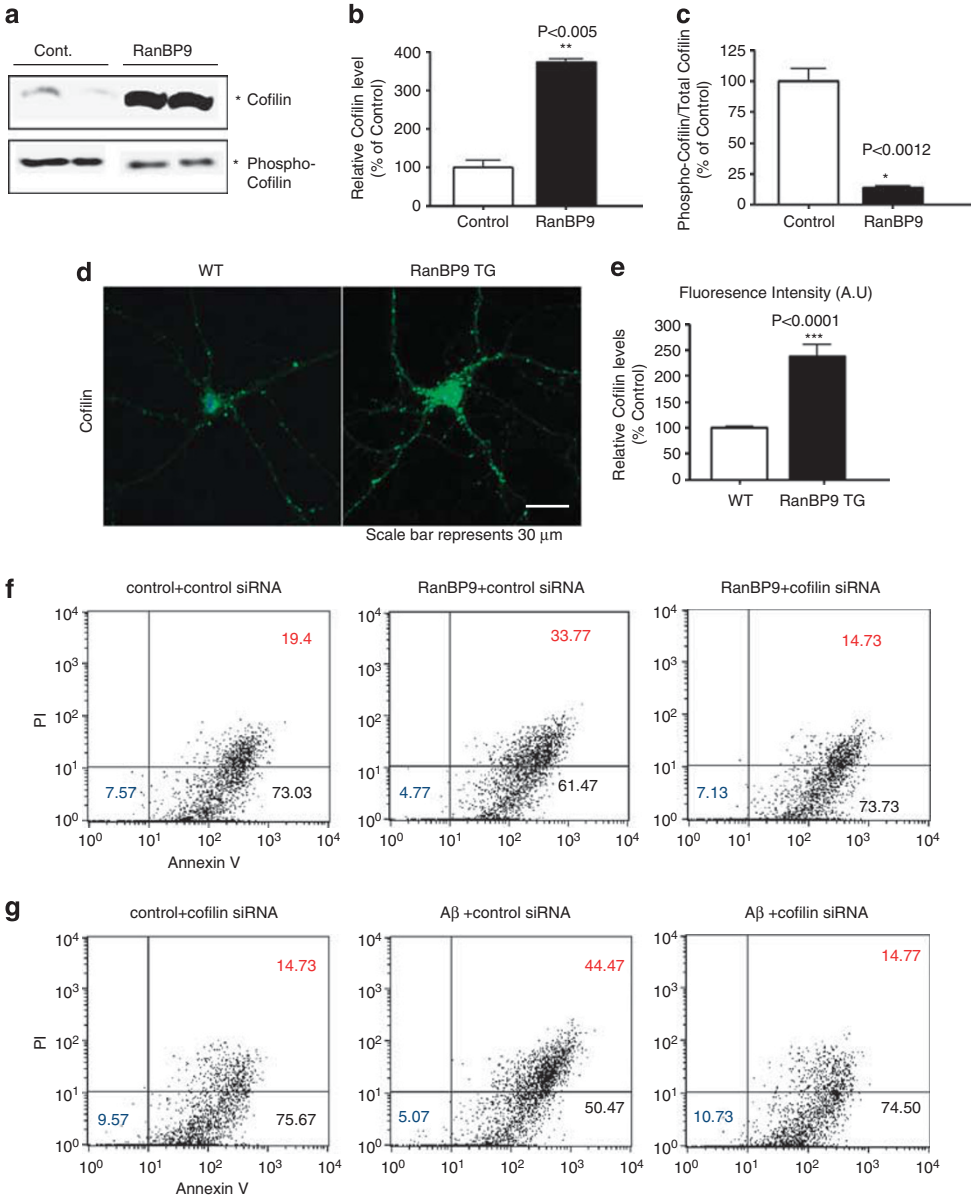

Figure 7 RanBP9 promotes cofilin activation, and cofilin is essential for Aβ and RanBP9-induced apoptosis. (**a**) NIH3T3 cells were transfected with vector control or RanBP9, and lysates were subjected to immunoblotting for cofilin and phospho-cofilin (serine-3). (**b** and **c**) Phospho-cofilin was divided by total cofilin levels ($n = 3$ each). Error bars represent S.E.M. (**d** and **e**) DIV21 hippocampal neurons derived from RanBP9 transgenic and wild-type littermate mice were subjected to immunofluorescence for cofilin. Intensity of cofilin immunofluorescence signal was quantitated from randomly selected neurons (at least 10 neurons from 3 wt and 3 RanBP9 transgenic mice). Error bars represent S.E.M. (**f** and **g**) HT22 cells were transfected with vector control or RanBP9 with or without with sense control siRNA or cofilin-specific siRNA (two siRNA transfections in 24 h). After the second siRNA transfection, the medium was replaced with 1% FBS-containing medium for 36 h in the presence or absence of 1 μM Aβ1–42. Cells were then subjected to FACS analysis after propidium iodide (PI: *Y*-axis) and Annexin V (*X*-axis) staining. Under these conditions, note that both RanBP9 and 1 μM Aβ1–42 increases the conversion of early apoptotic cells (lower right quadrant) to late apoptotic cells (upper right quadrant). However, transfection of cofilin siRNA completely abolishes this apoptotic process. A representative experiment is shown from three independent experiments

transgenic primary hippocampal neurons (Figures 7d and e). As previous studies have demonstrated that cofilin has an essential role in oxidant-induced cell death,[16] we next tested whether cofilin is required for RanBP9- and Aβ-induced apoptosis. Indeed, siRNA knockdown of cofilin (Supplementary Figure S6B) completely abolished the conversion of early to late apoptotic cell death induced by RanBP9 as well as by Aβ1–42 oligomers (Figures 7f and g). Taken together, these data indicate that RanBP9-mediated activation of cofilin is required for Aβ-induced cell death.

Discussion

Aβ deposition, synaptic damage, gliosis, and memory deficits encompass the pathophysiological features of AD. In this study, we made a series of novel observations implicating the RanBP9-cofilin pathway as a critical mediator of Aβ-induced apoptosis and neurodegenerative changes reminiscent of AD. Specifically, overexpression of mutant APP dramatically increased RanBP9 protein levels in transgenic mice. To test the hypothesis that RanBP9 might be pathogenic, we generated RanBP9 transgenic mice as an *in vivo* experimental model of increased RanBP9 expression. Indeed, RanBP9 transgenic mice demonstrated severely reduced synaptophysin and synapsin I immunoreactivities associated with markedly increased neurodegeneration and neuroinflammation within the hippocampus. Such changes in synapse loss were also evident in DIV21 RanBP9 transgenic neurons by both synaptophysin and PSD95 staining, indicating that both presynaptic and postsynaptic ends of the synapse are perturbed at an early phase. These neurodegenerative changes were correlated with severe deficits in hippocampus-dependent spatial learning and memory. RanBP9 also enhanced the vulnerability of HT22 cells to apoptosis and enhanced Aβ-induced cell death independent of its capacity to promote Aβ generation. Furthermore, reduction in endogenous RanBP9 protected HT22 cells and primary neurons from Aβ-induced apoptosis, indicating that RanBP9 is an essential intracellular mediator of Aβ-induced neurotoxicity. Importantly, RanBP9 strongly promoted cofilin activation, and cofilin was required for both RanBP9 and Aβ-induced cell death. Taken together, these findings implicate a critical role of the RanBP9-cofilin pathway in the pathogenic neurodegenerative changes seen in AD.

As predicted from our initial antibody array analysis, RanBP9 transgenic mice demonstrated robust microgliosis and astrocytosis, consistent with generalized degeneration of the hippocampus as evidenced by markedly increased TUNEL-positive-condensed nuclei. Interestingly, the major regions of synaptic loss as assessed by synaptophysin and synapsin I immunoreactivities were within the hilus and IML of the dentate gyrus (hilar mossy cell terminating zone) and SL of CA3 (granule cell-terminating zone). These synaptic terminating zones arise from the dentate gyrus, an adult neurogenic region. Specifically, new born neurons proliferate in the subgranular zone of the dentate gyrus, from which they migrate either into the granule cell layer or hilar region of the dentate gyrus and form functional connections.[17] Therefore, these data raise the intriguing possibility that the loss of proper neurogenesis in RanBP9 transgenic brains might at least in part account for the observed synapse loss seen within the SL of CA3 and hilus/IML of the dentate gyrus. Furthermore, the observation that RanBP9 transgenic mice are severely impaired in hippocampus-dependent spatial memory tasks functionally underscores the neuroinflammation, neurodegeneration, and synaptic loss seen in the hippocampus.

Multiple studies have shown that Aβ binds to various integrins, a process that is required for Aβ-induced neurotoxicity. Although integrin blocking antibodies or echistatin (a highly selective and potent integrin inhibitor) inhibit Aβ-induced neurotoxicity and LTP,[18,19] the signaling components of this inhibitory activity are unknown. Downstream of integrins, the assembly and disassembly of G-actin to F-actin is a process critical to many cellular processes, including cell motility, dendritic spine morphogenesis, membrane protein endocytosis, and cell death.[20] ADF/cofilin, a family of actin-binding protein, is perhaps one of the key regulators of actin dynamics and oxidant-induced cell death.[16,21] Dephosphorylated and oxidized cofilin loses its affinity for actin and translocates into the mitochondria where it induces cytochrome c release by promoting the opening of the permeability transition pore.[16] Interestingly, it has been shown that Aβ promotes cofilin–actin pathology, inclusions that contain dephosphorylated cofilin, actin, and hyperphosphorylated tau.[3,4] Moreover, Aβ oligomers induce defects in PAK signaling (a downstream component of integrin activation), leading to the activation/dephosphorylation of cofilin and synaptic pathology. Overexpression of active PAK reverses these effects of Aβ oligomers.[22,23] Cofilin also has a key role in the loss of dendritic spines induced by Aβ.[24] These observations all indicate that activation/dephosphorylation of cofilin is a key component of Aβ-induced neurotoxicity at multiple levels. Although RanBP9 has previously been implicated in the promotion of cell death, the mechanisms of such activity are unknown.[25] We have previously shown that RanBP9 accelerates APP, LRP, and β1-integrin endocytosis, simultaneously leading to increased Aβ generation *in vitro* and *in vivo*[6,7] and disruption of focal adhesions.[9] As such, our observation that RanBP9 activates/dephosphorylates cofilin is consistent with the known role of the integrin-LIMK pathway in the inactivation/phosphorylation of cofilin, although the Slingshot pathway cannot be ruled out. Therefore, we propose that disruption of cell adhesive processes via deregulation of integrin-dependent focal adhesions and activation of cofilin underlie both Aβ and RanBP9-induced increase in the vulnerability of neurons to undergo neuritic dysfunction, synapse loss, and mitochondria-mediated apoptotic process (Figure 8).[26] This hypothesis is supported by our observations that RanBP9 strongly promotes cofilin dephosphorylation/activation, and both RanBP9 and cofilin are essential for Aβ-induced cell death. The observation that the ability of RanBP9 to promote cell death is not dependent on its capacity to promote Aβ generation in our paradigm indicates that RanBP9 has three positively reinforcing roles in AD pathogenesis: (1) promotion of neurotoxicity on its own, (2) mediation of Aβ-induced neurotoxicity, and (3) promotion of Aβ generation (Figure 8). Taken together, these data strongly implicate the RanBP9-cofilin pathway in neurodegenerative processes downstream of Aβ accumulation.

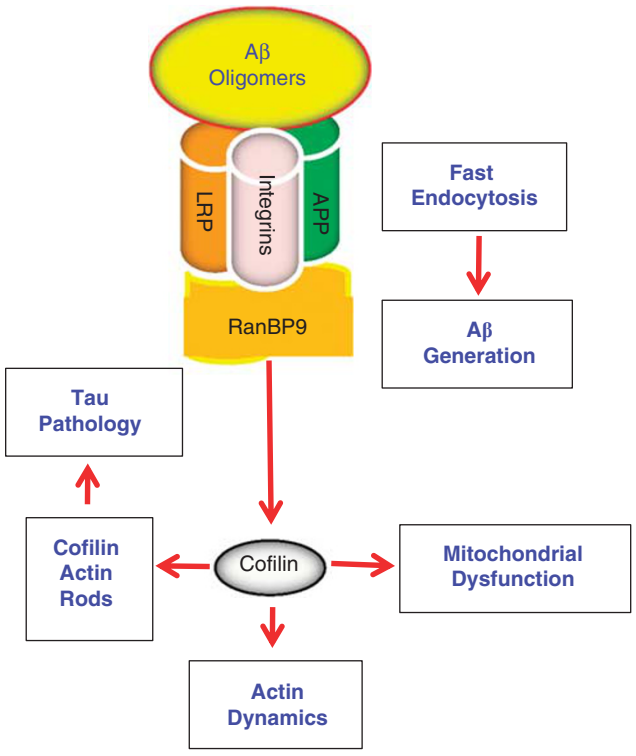

Figure 8 Schematic model of the RanBP9-cofilin pathway in AD pathogenesis. As the binding of Aβ to various integrins is critical to transmit its neurotoxic signals, Aβ oligomers are proposed to activate/dephosphorylate cofilin via the recruitment of RanBP9 to integrin/APP/LRP complexes. The binding of RanBP9 to integrin/APP/LRP complexes accelerates their endocytosis, thereby promoting Aβ generation, disrupting focal adhesions, and activating cofilin. Under conditions of oxidative stress such as that induced by Aβ oligomers, oxidized, and dephosphorylated cofilin translocates into the mitochondria to open up the mitochondrial permeability transition pore, which induces mitochondrial dysfunction and promotes apoptotic processes. Activated cofilin can lead to the formation of cofilin-actin rods, which attract hyperphosphorylated tau and promote tau pathology

Together with our previous demonstration that RanBP9 robustly enhances Aβ generation,[6–8] these data further implicate the RanBP9-cofilin pathway not only as therapeutic targets to stem Aβ generation but also block the neurotoxic effects of Aβ.

Materials and Methods

Plasmids, cell death assays, and transfections. Plasmids pLHCX Flag-RanBP9, p3X Flag-RanBP9, pEGFP-RanBP9, and pEYFP-N1 constructs have previously been described.[6,8] To examine the stage of apoptotic cells, the measurements were carried out using FACS Calibur (BD Bioscience, San Jose, CA, USA) or fluorescence microscopy. Cells were either trypsinized/collected stained in solution or directly on glass coverslips with Annexin V-fluorescein and PI for 20 min at 25 °C in the dark state using the FITC Annexin V apoptosis detection kit I (BD, San Diego, CA, USA). After washing with ice-cold PBS, cells were measured by flow cytometry or by fluorescence microscopy. Transfections were performed with Lipofectamine 2000 (Life technologies, Invitrogen, Carlsbad, CA, USA) according to the manufacturer's protocol for 24 h. The 19-nucleotide siRNA duplexes targeting RanBP9, 5′-tcttatcaacaatacctgc-3′,[6] and cofilin, 5′-GGAGGACCUGGUGUUCAUC-3′,[27] or single strand sense control siRNAs were transiently transfected at 50–100 nM final concentrations.

Immunofluorescence. Animals were perfused with 4% paraformaldehyde in PBS, and the brains were post-fixed in the same fixative for 24 h. The brains were then cryoprotected in 30% sucrose and sectioned (30 μm) coronally on a cryostat. Sections were washed with PBS and blocked with 3% BSA and 0.2% Triton X-100 in PBS for 30 min. The following primary antibodies were applied overnight: anti-Iba-1 (1 : 1000, Abcam); anti-activated GFAP (1 : 1000, Invitrogen); anti-synaptophysin (1 : 250, Sigma, St. Louis, MO, USA); and synapsin I (1 : 1000, Cell Signaling Technology, Beverly, MA, USA). After several washes with PBS, appropriate secondary antibodies (Life technologies, Molecular Probes, Carlsbad, CA, USA) were applied for 30 min. Subsequently the sections were washed, mounted, and observed under a fluorescence or confocal microscope (Olympus, Tokyo, Japan). GFAP and Iba-1 immunoreactive cells were counted in every 12th serial section through an entire hippocampus. The different hippocampal regions were identified by the density and the size of nuclei after counterstaining with Hoechst33342 (blue). Synaptophysin and synapsin I immunoreactivities were determined by quantifying the density of presynapses of SL of CA3 (granule cell mossy fiber terminating zone) and CA1 (CA3 Schaffer collateral terminating zone), and IML (hilar mossy cell terminating zone) of the dentate gyrus within the hippocampus of RanBP9 transgenic and WT mice using Image J software (National Institutes of Health, Bethesda, MD, USA). Secondary antibody background signal alone from the same region was subtracted from the total signal before comparison of samples.

Behavioral analyses. The Barne's maze used was an opaque Plexiglas disc 75 cm in diameter elevated 58 cm above the floor by a tripod. Twenty holes, 5 cm in diameter, were located 5 cm from the perimeter, and a black Plexiglas escape box ($19 \times 8 \times 7$ cm) was placed under one of the holes. Distinct spatial cues were located all around the maze and were kept constant throughout the study. On the first day of testing, a training session was performed that consisted of placing the mouse in the escape box and leaving it there for 1 min. One minute later, the first session was started. At the beginning of each session, the mouse was placed in the middle of the maze in a 10 cm high cylindrical black start chamber. After 10 s the start chamber was removed, a buzzer (80 dB) and a light (400 lux) were turned on, and the mouse was set free to explore the maze. The session ended when the mouse entered the escape tunnel or after 3 min elapsed. When the mouse entered the escape tunnel, the buzzer was turned off and the mouse was allowed to remain in the dark for 1 min. If the mouse did not enter the tunnel by itself it was gently put in the escape box for 1 min. The tunnel was always located underneath the same hole (stable within the spatial environment), which was randomly determined for each mouse. Mice were tested once a day for 12 days for the acquisition portion of the study. For the 13th test (probe test), the escape tunnel was removed and the mouse was allowed to freely explore the maze for 3 min. The time spent in each quadrant was determined and the percent time spent in the target quadrant (the one originally containing the escape box) was compared with the average percent time in the other three quadrants. This is a direct test of spatial memory as there is no potential for local cues to be used in the mouse's behavioral decision. In addition, the strategies used by the animals to perform the task were readily revealed.

For cued and contextual fear conditioning, conditioning took place in Freeze Monitor chambers (Med Associates) housed in sound proofed boxes. The conditioning chambers ($26 \times 26 \times 17$ cm) were made of Plexiglas with speakers and lights mounted on two opposite walls. The chambers were installed with a shockable grid floor. On day 1, mice were placed in the conditioning chamber for 5 min in order to habituate them to the apparatus. On day 2, the mice were exposed to the context and conditioned stimulus (30 s, 3000 Hz, 80 dB sound) in association with foot shock (0.70 mA, 2 s, scrambled current). Specifically, a 5.5-min session was run in which the mice received two shock exposures, both in the last 2 s of a 30-s tone exposure. On day 3, contextual conditioning (as determined by freezing behavior) was measured in a 5-min test in the chamber where the mice were trained (context test). On day 4, the mice were tested for cued conditioning (CS + test). The mice were placed in a novel context for 3 min, after which they were exposed to the conditioned stimulus (tone) for 3 min. For this test, the chamber was disguised with new walls (black opaque plastic creating a triangular-shaped compartment in contrast to a clear plastic square compartment), a new floor (black opaque plastic in contrast to metal grid), and a novel odour (drop of orange extract under the floor). Freezing behavior, that is, the absence of all voluntary movements except breathing, was measured in all sessions by a validated computer-controlled recording of photocell beam interruptions. Freezing behavior in the context and cued tests (relative to the same context prior to shock and an altered context prior to tone, respectively) was indicative of the formation of an association between the particular stimulus (either the environment or the tone) and the shock; that is, that learning has occurred.

Statistical analysis. Data were analyzed by Instat3 software (GraphPad Software, San Diego, CA, USA) using either Student's *t*-test or one-way analysis of variance (ANOVA) followed by a Neuman–Keuls *post hoc* test. Data were expressed as mean ± S.E.M. Differences were deemed significant when $P < 0.05$. The signal intensity from immunoblots was quantified using Image J software.

Conflict of Interest

The authors declare no conflict of interest.

Acknowledgements. We thank Dr. Amanda Roberts for valuable help with behavioral analysis, Dr. Elisabetta Bianchi for the RanBP9 monoclonal antibody, and Dr. Mark Ginsberg for helpful discussions. This work was supported in part by the American Health Assistance Foundation (A2007-05, DE Kang), NIH/NIA (1R01AG033055-01A1, DE Kang), NIH/NIA (1K02AG031920-10A1, DE Kang), WCU-Neurocytomics Project grant from NRF (DE Kang & I Mook-Jung), NIH/NIA (1R03AG032064-01, MK Lakshmana), and NIH/NIA (1R01AG036859-01, M.K. Lakshmana).

1. De Strooper B, Annaert W. Proteolytic processing and cell biological functions of the amyloid precursor protein. *J Cell Sci* 2000; **113** (Part 11): 1857–1870.
2. Bamburg JR, Bloom GS. Cytoskeletal pathologies of Alzheimer disease. *Cell Motil Cytoskeleton* 2009; **66**: 635–649.
3. Whiteman IT, Gervasio OL, Cullen KM, Guillemin GJ, Jeong EV, Witting PK *et al.* Activated actin-depolymerizing factor/cofilin sequesters phosphorylated microtubule-associated protein during the assembly of Alzheimer-like neuritic cytoskeletal striations. *J Neurosci* 2009; **29**: 12994–13005.
4. Davis RC, Marsden IT, Maloney MT, Minamide LS, Podlisny M, Selkoe DJ *et al.* Amyloid beta dimers/trimers potently induce cofilin-actin rods that are inhibited by maintaining cofilin-phosphorylation. *Mol Neurodegener* 2011; **6**: 10.
5. Yao J, Hennessey T, Flynt A, Lai E, Beal MF, Lin MT. MicroRNA-related cofilin abnormality in Alzheimer's disease. *PLoS One* 2010; **5**: e15546.
6. Lakshmana MK, Yoon IS, Chen E, Bianchi E, Koo EH, Kang DE. Novel role of RanBP9 in BACE1 processing of amyloid precursor protein and amyloid beta peptide generation. *J Biol Chem* 2009; **284**: 11863–11872.
7. Lakshmana MK, Hayes CD, Bennett SP, Bianchi E, Reddy KM, Koo EH *et al.* Role of RanBP9 on amyloidogenic processing of APP and synaptic protein levels in the mouse brain. *FASEB J* 2012; e-pub ahead of print 31 January 2012, doi: 10.1096/fj.11-196709.
8. Lakshmana MK, Chung JY, Wickramarachchi S, Tak E, Bianchi E, Koo EH *et al.* A fragment of the scaffolding protein RanBP9 is increased in Alzheimer's disease brains and strongly potentiates amyloid-beta peptide generation. *FASEB J* 2010; **24**: 119–127.
9. Woo JA, Roh SE, Lakshmana MK, Kang DE. Pivotal role of RanBP9 in integrin-dependent focal adhesion signaling and assembly. *FASEB J* 2012; e-pub ahead of print 5 January 2012, doi: 10.1096/fj.11-194423.
10. Mucke L, Masliah E, Yu GQ, Mallory M, Rockenstein EM, Tatsuno G *et al.* High-level neuronal expression of abeta 1–42 in wild-type human amyloid protein precursor transgenic mice: synaptotoxicity without plaque formation. *J Neurosci* 2000; **20**: 4050–4058.
11. Behl C, Widmann M, Trapp T, Holsboer F. 17-Beta estradiol protects neurons from oxidative stress-induced cell death *in vitro*. *Biochem Biophys Res Commun* 1995; **216**: 473–482.
12. Klein WL. Abeta toxicity in Alzheimer's disease: globular oligomers (ADDLs) as new vaccine and drug targets. *Neurochem Int* 2002; **41**: 345–352.
13. Wang HW, Pasternak JF, Kuo H, Ristic H, Lambert MP, Chromy B *et al.* Soluble oligomers of beta amyloid (1–42) inhibit long-term potentiation but not long-term depression in rat dentate gyrus. *Brain Res* 2002; **924**: 133–140.
14. Bernard O. Lim kinases, regulators of actin dynamics. *Int J Biochem Cell Biol* 2007; **39**: 1071–1076.
15. Eiseler T, Doppler H, Yan IK, Kitatani K, Mizuno K, Storz P. Protein kinase D1 regulates cofilin-mediated F-actin reorganization and cell motility through slingshot. *Nat Cell Biol* 2009; **11**: 545–556.
16. Klamt F, Zdanov S, Levine RL, Pariser A, Zhang Y, Zhang B *et al.* Oxidant-induced apoptosis is mediated by oxidation of the actin-regulatory protein cofilin. *Nat Cell Biol* 2009; **11**: 1241–1246.
17. Forster E, Zhao S, Frotscher M. Laminating the hippocampus. *Nat Rev Neurosci* 2006; **7**: 259–267.
18. Anderson KL, Ferreira A. Alpha1 integrin activation: a link between beta-amyloid deposition and neuronal death in aging hippocampal neurons. *J Neurosci Res* 2004; **75**: 688–697.
19. Wang Q, Klyubin I, Wright S, Griswold-Prenner I, Rowan MJ, Anwyl R. Alpha v integrins mediate beta-amyloid induced inhibition of long-term potentiation. *Neurobiol Aging* 2008; **29**: 1485–1493.
20. Bernstein BW, Bamburg JR. ADF/cofilin: a functional node in cell biology. *Trends Cell Biol* 2010; **20**: 187–195.
21. Chua BT, Volbracht C, Tan KO, Li R, Yu VC, Li P. Mitochondrial translocation of cofilin is an early step in apoptosis induction. *Nat Cell Biol* 2003; **5**: 1083–1089.
22. Zhao L, Ma QL, Calon F, Harris-White ME, Yang F, Lim GP *et al.* Role of p21-activated kinase pathway defects in the cognitive deficits of Alzheimer disease. *Nat Neurosci* 2006; **9**: 234–242.
23. Ma QL, Yang F, Calon F, Ubeda OJ, Hansen JE, Weisbart RH *et al.* p21-activated kinase-aberrant activation and translocation in Alzheimer disease pathogenesis. *J Biol Chem* 2008; **283**: 14132–14143.
24. Shankar GM, Bloodgood BL, Townsend M, Walsh DM, Selkoe DJ, Sabatini BL. Natural oligomers of the Alzheimer amyloid-beta protein induce reversible synapse loss by modulating an NMDA-type glutamate receptor-dependent signaling pathway. *J Neurosci* 2007; **27**: 2866–2875.
25. Atabakhsh E, Bryce DM, Lefebvre KJ, Schild-Poulter C. RanBPM has proapoptotic activities that regulate cell death pathways in response to DNA damage. *Mol Cancer Res* 2009; **7**: 1962–1972.
26. Kang DE, Roh SE, Woo JA, Liu T, Bu JH, Jung AR *et al.* The interface between cytoskeletal aberrations and mitochondrial dysfunction in Alzheimer's disease and related disorders. *Exp Neurobiol* 2011; **20**: 67–80.
27. Hotulainen P, Paunola E, Vartiainen MK, Lappalainen P. Actin-depolymerizing factor and cofilin-1 play overlapping roles in promoting rapid F-actin depolymerization in mammalian nonmuscle cells. *Mol Biol Cell* 2005; **16**: 649–664.

Supplementary Information accompanies the paper on Cell Death and Differentiation website (http://www.nature.com/cdd)